Research Article

SOHAG JOURNAL OF SCIENCES

https://doi.org/10.21608/sjsci.2025.321557.1223

Antimicrobial Agents Based on Novel imine Complexes Incorporating Pr(III), Nd(III) and Sm(III) Cations

Shimaa M. Abdel-Fatah[1,*], Laila H. Abdel Rahman[1], Mohamed R. Shehata[2]

[1] *Chemistry Department, Faculty of Science, Sohag University, Sohag, 82524, Egypt*
[2] *Chemistry Department, Faculty of Science, Cairo University, Giza, 12613, Egypt*
[*]*Email: shima_mahdi@science.sohag.edu.eg*

Received: 22nd September 2024, **Revised:** 16th November 2024, **Accepted:** 1st January 2025
Published online: 9th March 2025

Abstract: IR, TGA, UV/Vis, and ^{1}HNMR techniques together with powder X-ray diffraction, elemental (CHN) and mass spectra analysis, molar conductance, and magnetic susceptibility studies were utilized to synthesize and report novel imine-complexes of Pr(III); Nd(III) and Sm(III) cations. The conductivity measurements demonstrate that none of the complexes are electrolytes. Data of magnetic susceptibility support the paramagnetism of all lanthanide (III) complexes. Depending on various analyses, trivalent cations favor a 1:1 lanthanide: ligand. According to biological investigations, every complex demonstrated effective antimicrobial efficacy against a wide variety of bacterial and fungal strains. Additionally, we noticed that the Ln (III) complexes' antimicrobial potency was ordered as follows: NdA > PrA > SmA > H_2A. It was determined that the Nd(III) combination had the maximum inhibition zone (22 mm) and was the most efficient against Gram-negative bacteria. The antimicrobial effectiveness against fungus (A. Flavus) goes as follows: PrA > NdA > SmA > H_2A. The equilibrium geometry of the imine ligand and its complexes at the B3LYP level of theory, where (C, H, O, N, and Cl) atoms at 6-311G++(d, p) and Nd, Pr, and Sm at SDD, was clarified using density functional theory (DFT) calculations utilizing the Gaussian 09 program. Lastly, docking experiments have shown. Ultimately, this research aspires to contribute to developing novel metal-based drugs with enhanced therapeutic propereties.
Keywords: Complexes, Mass spectra, TGA, Magnetic susceptibility, Docking studies, Bacteria.

1. Introduction

Schiff bases are crucial for processes like (C-C) bond cleavage and transamination. Schiff bases play a significant part in living organisms, tial type of ligands for coordination chemistry is the imine, which coordinates to metal ions via (azomethine nitrogen) [1-7].

The usage of lanthanide elements and their derivatives are numerous. The lanthanides are crucial in catalysis and in the manufacture of glasses.

Methylacidiphilum fumariolicum; a bacterium from the phylum that has the enzyme methanol dehydrogenase, utilizes lanthanides as enzymatic cofactors . Only when lanthanides are present in the environment was it discovered that this bacterium may survive. Lanthanide which aren't radioactive, considered as having low poisoning [8-10].

Lanthanide ions and related substances have drawn both academic and industrial research due to their great medical usefulness [11–16]. On complexation with lanthanide metals/ions, it is discovered that many chemical compounds of physiological significance developed into more biologically active molecules [17–18].

Using Schiff base ligands, a variety of lanthanide complexes have been created with formula $[HNEt_3][LnL_x(NO_3)_2(H_2O)]H_2O$. The formula for these compounds was determined using different methods. In the enol tautomeric state, the metal ion coordinates through the phenolate (O), imine(N), and deprotonated amide(O) atoms. Due to the fact that the coordination environment surrounding the metal ion is carried out by one coordinated water molecule and two bidentate nitrate ligands, Ln(III) complexes have a coordination number of eight [19].

One pot technique was used to create 4-(anthracen-10-yl)-2,6-di(pyridin-2-yl) pyridine by condensation of [2-acetyl pyridine] and [anthracene-10-carbaldehyde] with ammonia. The synthesis of lanthanide complexes (La, Sm, and Eu) as a new prospective biological agent was carried out using this hybrid ligand. Molar conductivity, elemental, FT-IR, UV-visible, and mass spectrometry were used to characterize the lanthanide complexes. In vitro antimicrobial activity against Escherichia coli; Staphylococcus aureus and Aspergillus niger, were assessed for the complexes. [20].

Despite extensive research on metal complexes of Schiff bases, there is a lack of diverse metal ion exploration, comparative analyses, and detailed mechanistic insights. Therefore, in this work, we synthesize and thoroughly characterize a series of novel Ln(III) complexes, specifically Pr(III); Nd(III) and Sm(III) imine complexes, using a variety of analytical techniques. We evaluate these complexes' biological activities, focusing on their antimicrobial potential. Additionally, computational studies, including DFT calculations and molecular docking, are employed to gain deeper insights into the geometry and interaction mechanisms of the complexes with biological targets.

2. Materials and methods

2.1. Synthesis of imine ligand (H2A) and its Ln(III) -complexes

2.1.1.(2-[(5-Chloro-2-hydroxy-benzylidene)-amino]-pyridin-3-ol) (H2A).

5-chlorosalicylaldehyde (1 mmol, 0.156 g) was added up to 2-amino-3-hydroxypyridine (1.0 mmol, 0.110 g). The reaction mixture were stirred in ethanol for 45 min then refluxed at 60 ˚C for 2-3 h, filtered and washed with ethyl alcohol (H_2A); brown powder; yield, (82%); mp-185 ˚C; FTIR (cm^{-1}): 3219 (-OH), 1625 (C=N), 1286 (C-O $_{phenol}$). UV/ vis (λ_{max}): 258 nm, 399 nm. ^1H NMR (δ, ppm): 7.01-8.01 (m; 6H-Ar), 9.49 (s; 1H, CH=N), 10.24 (s; 1H, OH), 6.98 (s; 1H, OH); Mass (EI-MS): 248.33 (Calculated: 248.5) for $C_{12}H_9O_2N_2Cl$; Elemental analysis: C 57.61; H 3.76; N 11.36 (Calculated: C, 57.94; H, 3.62; N, 11.26).

2.1.2.(2-[(5-Chloro-2-hydroxy-benzylidene)-amino]-pyridin-3-ol) praseodymium (III) [PrA].

Ligand (H_2A) (1 mmol, 0.248 g) was added up to $PrCl_3{\cdot}6H_2O$ (1.0 mmol, 0.355 g). The reaction mix were refluxed in ethanol at 60 ˚C for 5 h, filtered and washed with ethanol; orange powder; yield, (76 %); mp-(>300) ˚C; FTIR (cm^{-1}): 3250 (H_2O_{hydr}), 1595(C=N), 1279(C-O $_{phenol}$), 900 (H_2O_{coord}), 550 (Ln-O), 488 (Ln-N), 431(Ln-Cl). UV/ vis (λ_{max}): 240 nm, 367 nm. Mass (EI-MS): 513.01 (Calculated: 512.9) for $C_{12}H_{17}O_7N_2Cl_2Pr$; Elemental analysis: C 28.33; H 3.02; N 5.49 (Calculated: C, 28.07; H, 2.92; N, 5.45). Λm ($\Omega^{-1}cm^2mol^{-1}$): 3.08; μ_{eff} (B.M):3.55.

2.1.3.(2-[(5-Chloro-2-hydroxy-benzylidene)-amino]-pyridin-3-ol) neodymium (III) [NdA].

Ligand (H_2A) (1 mmol, 0.248 g) was added up to $NdCl_3{\cdot}6H_2O$ (1.0 mmol, 0.358 g). The reaction mix were refluxed in ethanol at 60 ˚C for 5 h, filtered and washed with ethanol; orange powder; yield, (71 %); mp-(>300) ˚C; FTIR (cm^{-1}): 3309 (H_2O_{hydr}), 1607(C=N), 1293(C-O $_{phenol}$), 928 (H_2O_{coord}), 598 (Ln -O), 478 (Ln -N), 421(Ln-Cl). UV/ vis (λ_{max}): 236, 308 nm, 370 nm. Mass (EI-MS): 516.09 (Calculated: 516.2) for $C_{12}H_{17}O_7N_2Cl_2Nd$; Elemental analysis: C 28.13; H 3.09; N 5.60 (Calculated: C, 27.89; H, 2.90; N, 5.42). Λm ($\Omega^{-1}cm^2mol^{-1}$): 1.47; μ_{eff} (B.M):3.60.

2.1.4.(2-[(5-Chloro-2-hydroxy-benzylidene)-amino]-pyridin-3-ol) samarium (III) [SmA].

Ligand (H_2A) (1 mmol, 0.248 g) was added up to $SmCl_3{\cdot}6H_2O$ (1.0 mmol, 0.364 g). The reaction mix were refluxed in ethanol at 60 ˚C for 5 h, filtered and washed with ethanol; red powder; yield, (67 %); mp-(>300) ˚C; FTIR (cm^{-1}): 3233 (H_2O_{hydr}), 1597(C=N), 1291(C-O $_{phenol}$), 916 (H_2O_{coord}), 525 (Ln -O), 464 (Ln-N), 425(Ln-Cl). UV/ vis (λ_{max}): 252, 337 nm. Mass (EI-MS): 540.22 (Calculated: 540.3) for $C_{12}H_{19}O_8N_2Cl_2Sm$; Elemental analysis: C 26.42; H 3.01; N 5.33 (Calculated: C, 26.65; H, 2.77; N, 5.18). Λm ($\Omega^{-1}cm^2mol^{-1}$): 11.86; μ_{eff} (B.M):1.76, Scheme 1.

2.2. Physical characterization

2.2.1. Equipments

The melting point was determined via Gallenkamp apparatus, UK; Shimadzu FTIR spectrophotometer was used to capture their IR spectra (model 8101); whereas acetonitrile was used as solvent to assess their UV-visible (Uv-Vis) spectra using PG spectrophotometer; model T+80. 1H NMR and 13C NMR spectra were obtained using DMSO-d6 and a Bruker instrument operating at (400 MHz) with TMS serving as an internal standard. Jenway conductivity meter with model 4320 was utilized in DMF to assess conductivity. A thermogravimetric test was conducted using a Shimaduz Corporation 60H analyzer under N2, with a rate of heat {10 °C min^{-1}}.

Perkin-Elmer Elemental analyzer (model 240c) at Cairo University was employed for elemental analysis; Measure of the magnetic properety was made using Gouy's balance. The Microanalytical Center; National Research Center, Cairo, Egypt, performed mass spectra utilizing the EI technique were performed at 70 Ev using a Hewlett-Packard {MS-5988 GS-MS} apparatus and pH measurements carried out at 298 K using a HANNA 211 pH meter. The values of absorbance of 1×10^{-3} M of each complex were measured at various pH. The pH values were checked by using a series of Britton universal buffers. Using an X-ray diffractometer, the crystal structure was investigated. PANalytical's model X'pert3-Powder was employed, which uses monochromatized CuK radiation to get the crystal structure.

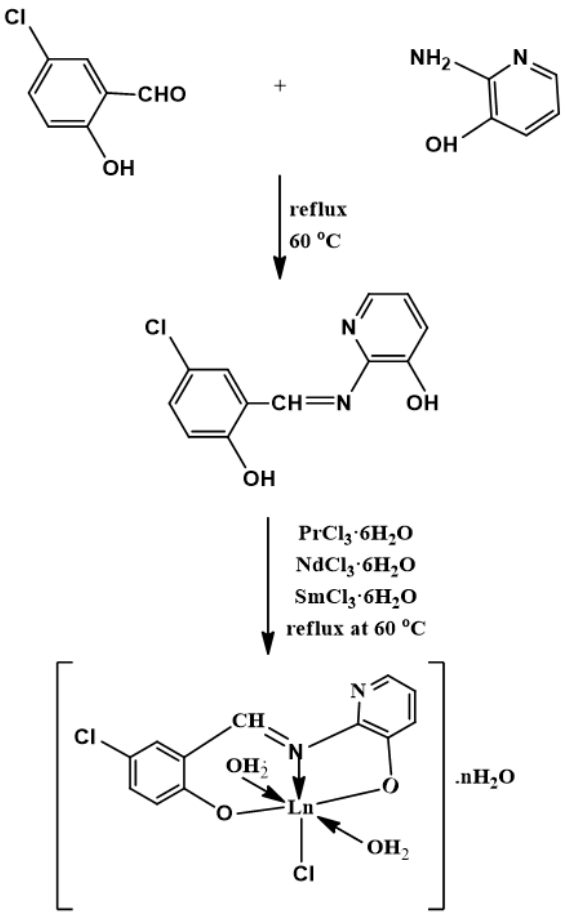

Scheme 1. Structure of complexes with tri-valent cations (M(III) = Pr, Nd, and Sm)[n=3 for Pr, Nd ; n=4 for Sm].

2.2.2. Chemicals

All the chemicals utilized in this study such as 5-Chlorosalicylaldehyde, 2-amino-3-hydroxypyridine, the metal salts such as ($PrCl_3 \cdot 6H_2O$, $NdCl_3 \cdot 6H_2O$ and $SmCl_3 \cdot 6H_2O$) were obtained from Sigma–Aldrich Chemie (Germany). Spectroscopic grade ethanol, DMSO (Dimethylsulfoxide) and DMF (Dimethylformamide) were used.

2.3. Antimicrobial potency

The antibacterial and antifungal efficacy of imine ligand and its lanthanide complexes (at 20 mg/ml concentration in DMSO) were assessed using the paper disc procedure. The minimum inhibitory concentration (MIC) was determined [21-25]. Ofloxacin was utilized as an antibacterial agent and Fluconazole was utilized as an antifungal agent.

2.4. Computational aspects

The Gaussian 09 software was utilized for all computations at the {B3LYP} level of theory. The ligand and desired complex geometries were computed by taking into account the atoms of {C, H, N, O, and Cl} at 6-311G++(d, p); (Nd, Pr and Sm) at SDD [26].

2.5. Molecular docking

The molecular docking was accomplished utilizing MOE2022 software, to find the potential binding mechanisms for the bacterium and fungal receptor's most active site of Aspergillus flavus (PDB ID: 1R4U) and Micrococcus luteus (PDB ID: 6KQ9) [27].

3. Results and Discussion:

3.1. Physicochemical properties

All the lanthanide (III) complexes are most commonly soluble in organic solvents, as DMSO. Data of magnetic susceptibility support the paramagnetism of all lanthanide (III) complexes. The conductivity measurements demonstrate that none of the complexes are electrolytes. Depending on various analyses, trivalent cations favor a 1:1 lanthanide: ligand. ^{1}H NMR spectra refers to formation Schiff base [28-30].

3.1.1. Infrared spectroscopy

In the IR spectra obtained for the (H_2A) ligand, the azomethine group is responsible for the ligand's sharp band at 1625 cm^{-1}. The spectrum also includes characteristic IR band at 1288 cm^{-1}, consistent with the existence of phenolic {C–O} group, The complexation with the azomethine (H-C=N) group is expected to result in an intense band in the extent of 1595–1607 cm^{-1} in all of the lanthanide (III) complexes; that confirm complexation between ligand and lanthanide ions. It's significant that all the Ln (III) complexes exhibit comparatively prominent IR bands between 900 and 928 cm^{-1}, which are explained by the existence of coordinated water molecules. The IR bands detected at 464-488, 525-598 and 421-431 cm^{-1}, which can be assigned to both {Ln-N} and {Ln-O} stretching vibrations and (Ln-Cl), respectively, were used to determine the presence of lanthanide ions in these complexes, as shown in Figure (1, S1) [31-32].

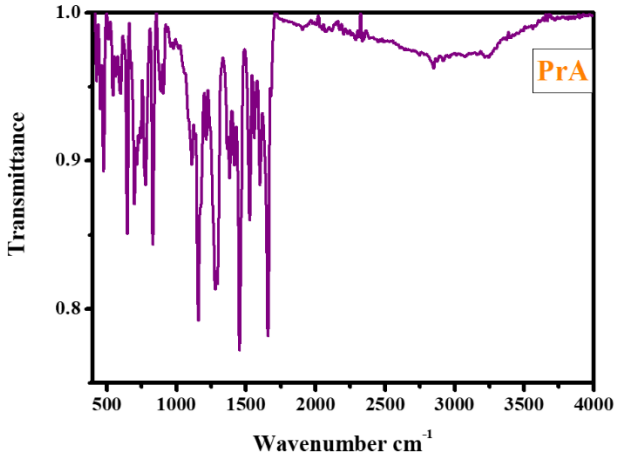

Figure 1: FT-IR spectra of PrA complex.

3.1.2. 1HNMR and 13CNMR of the prepared imine ligand

The ^{1}H-NMR spectra of the imine ligand show signals at (7.01-8.01; (m) δ), for aromatic protons and (9.49; (s) δ), for proton of the azomethine; that confirm the formation of imine. The peaks at (10.24 (s), 6.98 (s) δ) are resulted from –OH groups [33-34]. The ^{13}C-NMR spectra of the imine ligand show signals at (150.84 ppm), for azomethine carbon, (125.02-148.32 ppm) for aromatic carbons, as shown in Figure S2.

3.1.3. Electronic spectra

Electronic spectra of (H_2A) ligand displays an absorption band at ~299 nm, which is attributed to the π-π* transition, and an absorption band at ~470 nm, that is assigned to the n-π* transition. Lanthanide complexes show absorption band at 370–484 nm, which confirms the transfer of electrons from the ligand to the lanthanide which caused by the complexation of the nitrogen atom to the lanthanide ions. The significant changes in optical density for complexes in comparison to the ligand support the coordination between (H_2A) ligand and Ln(III) ions in the prepared complexes. Furthermore, the measured paramagnetic properties of the trivalent Ln -Schiff base (LnA) complexes correlate very well with their electronic spectra, as shown in Figure 2 [35].

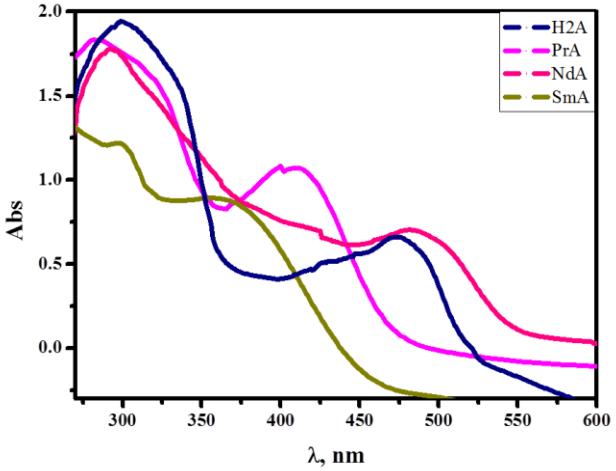

Figure 2: Electronic spectra of the prepared (H_2A) and its Ln(III) complexes.

3.1.4. Thermal Analysis

Thermal test was implemented under N_2 with a rate of heating 10 °C min^{-1}. The thermal degradation was happened in three stages (removal of water molecules of hydration then coordinated water molecules and finally removal of organic moiety). The PrA, NdA and SmA possess weight wastages of 13.78, 10.21 and 13.02 % respectively, that are resulted from loss of hydrated water molecules. The weight wastages of (10.65-41.96 %) coinciding to the loss of the residual fraction of the complex at {289-999 °C} for PrA complex. The weight wastages of (7.23-48.53 %) coinciding to the loss of the residual fraction of the complex at {146-999 °C} for NdA complex. The weight wastages of (20.11-32.97 %) coinciding to the loss of the residual fraction of the complex at {400-999 °C} for SmA complex, Table S1 and Figure S3[27]. The final product manifested from a horizontal curve has been gained proposing forming of metal oxide.

3.1.5. Kinetic aspects for TGA of the prepared imine complexes

The thermodynamic parameters of the decay process of the complexes were estimated by the Coats-Redfern equation (1). The activation entropy that has negative value indicates that the complexes were more organized than the reactant and the reactions were slow as shown in Table S2. Positive values were discovered for H* and G* respectively; standing for endothermic feature for all steps.

$$\log\left[\frac{\log w_\infty/(w_\infty - w))}{T^2}\right] = \log\left[\frac{AR}{\phi E^*}\left(1-\frac{2RT}{E^*}\right)\right] - \frac{E^*}{2.303RT} \quad (1)$$

Where W_∞ is the mass loss at the completion of the decomposition process. W is the mass loss up to temperature T, R is the gas constant and ϕ is the heating rate.

3.1.6. Mass spectra

The elemental analysis results and the observed molecular ions peaks are in good coincidence. For (H_2A) ligand, in terms of a molecular ion peak $[M]^+$ at 248.33 m/z, which is compatible with the estimated molecular weight of the $C_{12}H_9O_2N_2Cl^{35}$, the mass spectra of the (H_2A) ligand validated its stoichiometry; however, (H_2A) ligand exhibit $[M+2]^+$ isotopic peak at m/z 250.12 as a result for presence of Cl^{37} isotope, Figure S4. For Pr complex, in terms of a molecular ion peak $[M]^+$ at 513.01 m/z, which is compatible with the estimated molecular weight of the $C_{12}H_{17}O_7N_2Cl_2Pr$ complex, the mass spectra of the Pr complex supported its stoichiometry; however, Pr complex exhibit $[M+1]^+$ and $[M+2]^+$ isotopic peaks at m/z 513.73 and 514.33 . Pr complex exhibit isotopic peaks (3:1) at m/z 476.71 and 478.74 as a result for presence of $C_{12}H_{13}O_5N_2(Cl_2)^{35}Pr$, $C_{12}H_{13}O_5N_2(Cl_2)^{37}Pr$ (Figure 3). Nd and Sm complexes display several isotopes. For Nd complex, in terms of a molecular ion peak $[M]^+$ at 516.09 m/z, which is compatible with the estimated molecular weight of the $C_{12}H_{17}O_7N_2Cl_2Nd$ complex, the mass spectra of the Nd complex supported its stoichiometry; however, Nd complex exhibit $[M+2]^+$ and $[M+4]^+$ isotopic peaks at m/z 518.71 and 520.13. Nd complex exhibit isotopic peaks (3:1) at m/z 444.11 and 446.15 as a result for presence of $C_{12}H_9O_3N_2(Cl_2)^{35}Nd$, $C_{12}H_9O_3N_2(Cl_2)^{37}Nd$. For Sm complex, in terms of a molecular ion peak at 540.22 m/z, which is compatible with the estimated molecular weight of the $C_{12}H_{19}O_8N_2Cl_2Sm$ complex, the mass spectra of the Sm complex supported its stoichiometry; however, Sm complex exhibit $[M+2]^+$ and $[M+4]^+$ isotopic peaks at m/z 542.88 and 544.79 [36]. Sm complex exhibit isotopic peaks (3:1) at m/z 486.23 and 488.26 as a result for presence of $C_{12}H_{13}O_5N_2(Cl_2)^{35}Sm$, $C_{12}H_{13}O_5N_2(Cl_2)^{37}Sm$ and that refers to presence of (Ln-Cl).

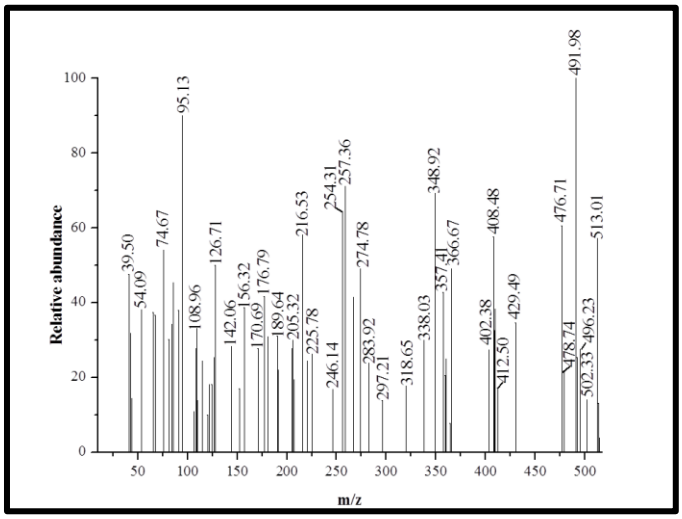

Figure. 3: Mass spectra of PrA complex.

3.1.7. PXRD Analysis

The crystal structure was investigated using XRD for (LnA) complexes. The spectra of lanthanide complexes showed no clearly defined crystalline peak, supporting the idea that the complexes have amorphous nature. The unit cell of (H_2A) ligand had lattice constants, a = 9.34820 Å; b = 7.04930 Å; c = 18.09240 Å; and unit cell volume V = 1192.26 $Å^3$. In light of these cell properties, a requirement for an orthorhombic sample, such as {a ≠ b ≠ c and α = β = γ = 90} was inspected, Figure 4 [37].

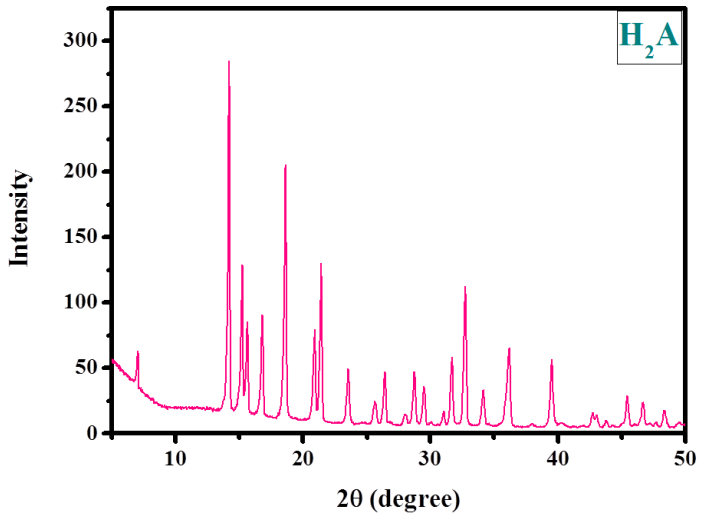

Figure. 4: PXRD pattern for H_2A ligand.

3.1.8. Electronic absorption spectra of the prepared imine complexes at different pH values

The absorbance vs. pH (pH-profile) depicted in Figure (S5) displayed a high stability pH range along with typical dissociation curves. This indicates that the imine ligand is significantly stabilized upon complex formation. Thus, the pH range of pH = 4 to pH = 10 is appropriate for the different fields of the complexes that have been studied.

3.2. Antimicrobial activity

The inhibition zone (mm); which is presented in Table S3, was measured in order to assess the antimicrobial potency. The standards used for the antibacterial and antifungal tests were ofloxacin and fluconazol, respectively. We also observed that the antimicrobial potency of the Ln(III) complexes was on the order of NdA > PrA > SmA > H_2A. It was determined that the NdA combination had the maximum inhibition zone (22 mm) and was the most efficient against Gram-negative bacteria. Chelation theory and the Overtone's concept were used to illustrate this phenomenon. The donor atoms in the ligand share some of the positive charge of the Ln(III) ion in a complex, causing electron delocalization throughout the entire chelated ring. As a result, the bacterial membrane's lipoid layers increased.

The order of increasing antimicrobial potency for the remaining compounds against fungi (A. Flavus) follows the order: PrA > NdA > SmA > H_2A which are presented in Figure 5. This research demonstrated that the prepared compounds have high biological activity and could effectively combat diseases. The results of this research are superior to those of previous studies [38-40].

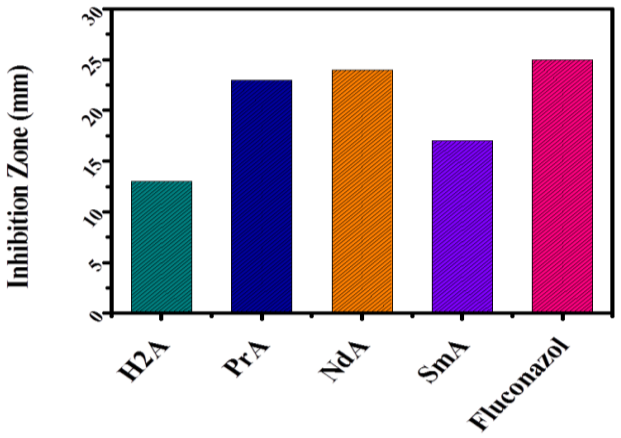

Figure.5: The zone of inhibition and activity index for the prepared (H_2A) and its Ln(III) complexes against (*A. Flavus*)

3.3. Molecular DFT Calculation

Figure 6 presents the optimized structures of H_2A as the lowest energy configurations. The natural charges got from Natural Bond Orbital Analysis (NBO) show that the active sites which more negative are N1{(-0.527), N2 (-0.468), O1 (-0.670), and O2 (-0.668)}. The metal ions prefer tridentate complexation to N1, O1, and O2 forming a 6-membered ring. Figure S6 displays the optimized lowest energies structures of the complexes [$NdA(H_2O)_2Cl$], [$PrA(H_2O)_2Cl$], and [$SmA(H_2O)_2Cl$], respectively. The metal atoms form six-coordinated in distorted octahedral geometries. The atoms (O1, N1, O2 and *Cl*2) are in one plane deviated by -0.003°, 0.000°, and 0.000°, in the complexes [$NdA(H_2O)_2Cl$], [$PrA(H_2O)_2Cl$] and [$SmA(H_2O)_2Cl$], respectively.

The distance between N1 and O1 decreased upon complex forming from 2.692Å in the free ligand to 2.123, 2.202, and 2.134Å in the complexes [$NdA(H_2O)_2Cl$], [$PrA(H_2O)_2Cl$] and [$SmA(H_2O)_2Cl$], respectively.

The distance between N1 and O2 decreased upon complex forming from 4.064Å in the free ligand to 2.314, 2.254 and 2.369Å in the complexes [$NdA(H_2O)_2Cl$], [$PrA(H_2O)_2Cl$] and [$SmA(H_2O)_2Cl$], respectively.

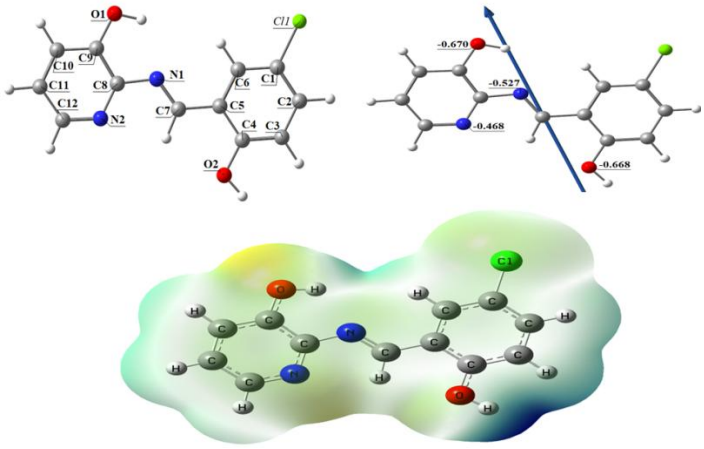

Figure. 6: The optimized structures of the ligand, the vector of the dipole moment, the natural charges on atoms and MEP (molecular electrostatic potential) surface by density function B3LYP/6-311++g(d,p).

The predicted total energy for the ligands and complexes was presented as well as the dipole moment, lowest unoccupied molecular orbital (LUMO) and highest occupied molecular orbital (HOMO) energies. Because of the ligand's chelation to metal ions, the complexes have narrower energy gaps [$(Eg)=E_{LUMO} - E_{HOMO}$] than the ligand. These more negative values of the complexes' total energy than the free ligand imply that the complexes are more stabilized than the free ligands. Figure 7 illustrates how the charge transfer interactions during compound formation are clarified by the reduction of Eg in complexes comparative to ligand.

Several reactivity descriptors have been proposed to comprehend various aspects of reactivity associated to chemical reactions [41]. These include ionization potential (I), electron affinity (A), electronegativity (χ), chemical potential (μ), hardness (η), softness (S), and electrophilicity index (ω). All of these reactivity descriptors are derived from the HOMO and LUMO energies, Tables S4, S5.

3.4. Molecular Docking

The binding free energy of the ligand and complexes with the receptor *Aspergillus flavus* (PDB ID: 1r4u) are found to be -5.2, -23.7, -22.0 and -12.3 kcal/mol for the ligand, [$NdA(H_2O)_2Cl$], [$PrA(H_2O)_2Cl$] and [$SmA(H_2O)_2Cl$] complexes; respectively, Table S6. The more negative the binding energy the more potent interaction.

[$NdA(H_2O)_2Cl$] > [$PrA(H_2O)_2Cl$] > [$SmA(H_2O)_2Cl$] > H_2A. The interaction of the [$NdA(H_2O)_2Cl$] complex with the active

site for the receptor of *Aspergillus flavus* (PDB ID: 1R4U) are presented in Figure 8.

The binding free energy of the ligand and complexes with the receptor of *Micrococcus luteus* (PDB ID: 6KQ9) are found to be -4.2, -33.0, -22.5 and -12.5 kcal/mol for the ligand, $[NdA(H_2O)_2Cl]$, $[PrA(H_2O)_2Cl]$ and $[SmA(H_2O)_2Cl]$ complexes; respectively, Table S7. The more negative the binding energy the more potent interaction.

$[NdA(H_2O)_2Cl] > [PrA(H_2O)_2Cl] > [SmA(H_2O)_2Cl] > H_2A$

The interaction of the $[NdA(H_2O)_2Cl]$ complex with the active site for the receptor of *Micrococcus luteus* (PDB ID: 6KQ9) are presented in Figure 9 [42].

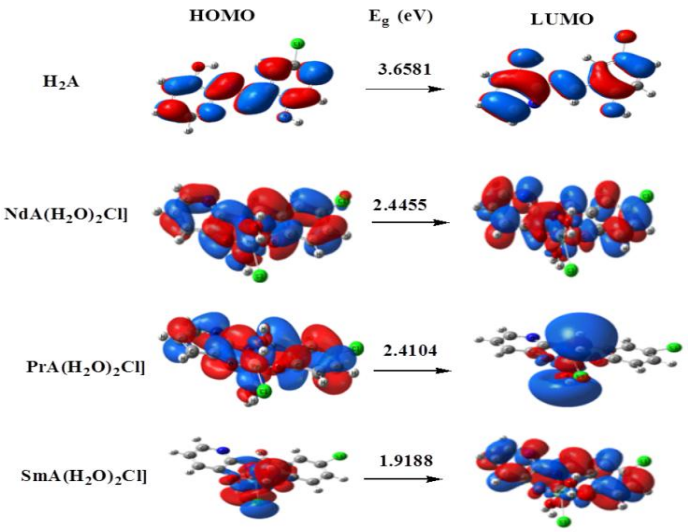

Figure.7: Maps of HOMO and LUMO charge density for the ligand, $[NdA(H_2O)_2Cl]$, $[PrA(H_2O)_2Cl]$ and $[SmA(H_2O)_2Cl]$ complexes.

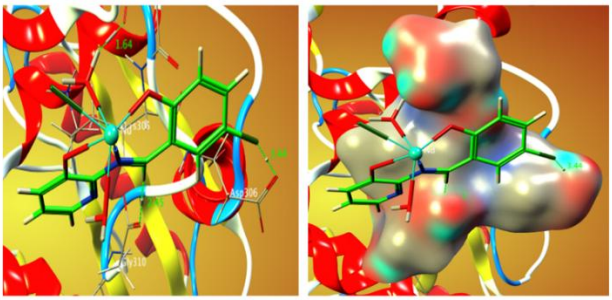

Figure.8: 3D plots of the interaction between NdA complex and the active site for the receptor of *Aspergillus flavus* (PDB ID: 1R4U).

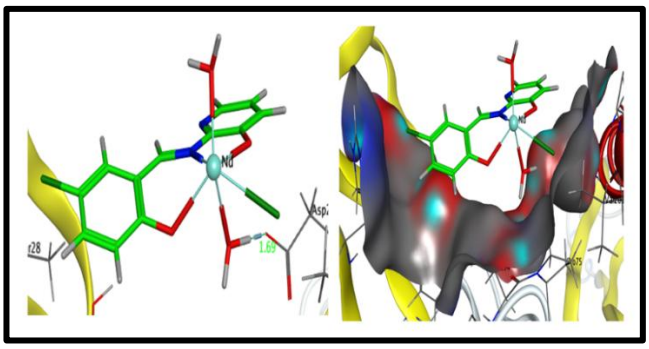

Figure. 9: 3D plots of the interaction between NdA complex and the active site for the receptor of *Micrococcus luteus* (PDB ID: 6KQ9).

4. Conclusion

In this work, a novel Schiff base (H2A) and its (Pr(III), Nd(III), and Sm(III)) imine complexes were synthesized and characterized using a range of analytical methods. The structure and composition were confirmed through the use of NMR spectroscopy, FTIR, elemental analysis, and mass spectra. None of the complexes are electrolytes, as shown by the conductivity measurements. Every lanthanide (III) complex exhibits paramagnetism propereties, according to magnetic susceptibility data. Depending on various analyses, trivalent cations favor a 1:1 lanthanide: ligand. Additionally, all Ln(III) complexes exhibit remarkable inhibitory potency against the tested bacterial and fungi strains in their biological activities compared to free ligand. The findings from this research suggest that the synthesized metal-imine complexes possess therapeutic propereties. Using novel metal-based drugs as anticancer and anti-inflammatory agents was recommended.

CRediT authorship contribution statement:

Conceptualization, L.A., S.A.; methodology, , L.A., S.A.; software, , L.A., S.A., M.S.; validation, , L.A., S.A., M.S.; formal analysis, , L.A., S.A., M.S.; investigation, , L.A., S.A.; resources, L.A., S.A.; data curation, S.A.; writing—original draft preparation, S.A.; writing—review and editing, L.A.; visualization, L.A., S.A., M.S.; supervision, L.A., S.A., M.S.; project administration, L.A., S.A., M.S.; funding acquisition, L.A., S.A.

Data availability statement

The data used to support the findings of this study are available from the corresponding author upon request.

Declaration of competing interest

The authors declare that they have no known competing financial interests or personal relationships that could have appeared to influence the work reported in this paper.

References

[1] H. Schiff, *Ann. Suppl.* 343(1864)1864-1865.
[2] S.S. Hassan, N.M. Rizk, M.A. Khidr and S.A. Aly, *Appl. Organo. Chem.* 38(2024)7298.
[3] A. Kajal, S.Bala, S.Kamboj, N.Sharma, V. Saini, *J. Catal.* 2013 (2013)1-14.
[4] P.A. vigato, S.Tamburini, *Coord. Chem. Rev.* 248(2004)1717-2128.
[5] P. Pfeiffer, E. Bucholz, O. Bouer, *J. Prakt. Chem.* 129(1931)163-177.
[6] P. Pfeiffer, E. Brieith, E. Lubbe, T.Tsumaki, J. Leibigs, *Ann. Chem.* 503(1933)84-130.
[7] P. Pfeiffer, H. Pfitzinger, *J. Prakt. Chem.* 145(1936)243-256.
[8] I. McGill, Rare earth elements. Ullm. Encycl.Indus. Chem. 2000.
[9] *A. Pol, et al . Environ. Microbiol.* 16(2014)255-264.
[10] A. Sigel, E. Freisinger, R.K. Sigel, Metal ions in bio-imaging techniques. Walter de Gruyter GmbH Co KG, 2021.
[11] Jr. Cotruvo, A. Joseph, *ACS cen. sci.* 5(2019)1496-1506.
[12] T. Cheisson, E. J. Schelter, *Science,* 363(2019)489-493.
[13] K. R. Long, B. S. Van Gosen, N. K. Foley, D. Cordier, *Springer Netherlands* (2012)131.
[14] D. Prodius, M. Klocke, V. Smetana, T. Alammar, M.P. Garcia, T.L. Windus, I.C. Nlebedim, A.V. Mudring, *Chem. Communi.* 56 (2020)11386-11389.

[15] Jr. Cotruvo, A. Joseph, R. F. Emily, A. M. Joseph, V. H. Jackson, N. L. Tatiana, *J Am. Chem. Soc*. 140(2018)15056-15061.
[16] J. A. Bogart, B. E. Cole, M. A. Boreen, C. A. Lippincott, B. C. Manor, P. J. Carroll, E. J. Schelter, *Proc. Natl. Acad. Sci. U. S. A.* 113(2016)14887-14892.
[17] H. Fang, B. E. Cole, Y. Qiao, J. A. Bogart, T. Cheisson, B. C. Manor, P. J. Carroll, E. J. Schelter, *Angew. Chem., Int. Ed.* 129 (2017)13635-13639.
[18] X.-Z. Li, L.-P. Zhou, L.-L.Yan, Y.-M. Dong, Z.-L. Bai, X.-Q. Sun, J. Diwu, S. Wang, J.-C. Bünzli, Q.-F. Sun, *Nat. Commun*. 9 (2018)547.
[19] Z. A. Taha , T. S. Ababneh, A. K. Hijazi, S. M. AL-Aqtash, W. M. Al-Momani, I. Mhaidat , *J. Saud. Chem. Soc.* 26(2022)101400.
[20] N. Nagaraju , J. Sreeramulu , V. Anjaneyulu , P. Malleswarareddy and G. Ramamohan, *Res. J. Chem. Environ*, 27(2023)42-51.
[21] NCCLS., Methods for Anti-Microbial Dilution and Disk Susceptibility Testing of Infrequently Isolated or Fastidious Bacteria; Approved Guideline Document M45-A. National Committee for Clinical Laboratory Standrd., Villanova PA USA, 26(1999).
[22] N.P. Priya, S.V. Arunachalam, N. Sathya, V. Chinnusamy, C. Jayabalakrishnan, *Transition Met. Chem*. 34(2009)437-445.
[23] A.A.A. Emara, *Spectrochim. Acta, Part A*, 77(2010)117-125.
[24] S. Jain, R. Sharma, V. Jain, R.C. Jat, S. Dubey, S. Bhardwaj, *J. Pharm. Res*. 3(2010)274.
[25] A.W. Bauer, W.M.M. Kirby, J.C. Sherris, M. Turck, *Am. J. Clin. Pathol*. 45(1966)493.
[26] T. Schaefer, R. Sebastian, G.H. Penner, S.R. Salman, *Can. J. Chem*. 64(1985)1602.
[27] C.C.G. Inc, "Molecular operating environment (MOE 2022.02)" Chemical Computing Group Inc. 1010 Sherbooke St. West, Suite # 910, Montreal, QC, Canada, H3A 2R7, (2022).
[28] W.J. Geary, *Coord. Chem. Rev*. 7(1971)81.
[29] P.K. Radhakrishnan, *Inorg. Chim. Acta*, 110(1985)211.
[30] W. Plass, G. Fries, Z. Anorg. *Allg. Chem*. 623(1997)1205.
[31] K. Mohanan, S.N. Devi, *Russ. J. Coord. Chem*. 32(2006)600.
[32] K. Mohanan, C.J. Athira, Y. Sindhu, M.S. Sujamol, *J. Rare Earths*. 27(2009)705.
[33] K. Kumar, S. Murugesan, T. Muneeswaran, C. Ramakritinan, *Cur. Chem. Lett*. 12(2023)721.
[34] A. Cinarli, D. Gurbuz, A. Tavman, A.S. Birteksz, *Bull. Chem. Soc. Ethiop*. 25(2011)407.
[35] A. Matwijczuk, D. Karcz, R. Walkowiak, J. Furso, B. Gładyszewska, S. Wybraniec, A. Niewiadomy, G.P. Karwasz, M. Gagos´, *J. Phys. Chem. A*, 121(2017)1402.
[36] G. Xu, Z.-M. Wang, Z. He, Z. Lu, C.-S. Liao, C.-H. Yan, *Inorg. Chem*. 41(2002)6802.
[37] C.J. Dhanaraj, M.S. Nair, *Eur. Polym. J*. 45(2009)565.
[38] M.T. Kaczmarek, M. Zabiszak, M. Nowak, R. Jastrzab, *Coord. Chem. Rev*. 370(2018)42.
[39] Y. Anjaneyula, R.P. Rao, *Synth. React Inorg. Met-Org. Chem*. 16 (1986)257.
[40] B.G. Tweedy, *Phytopathology*, 55(1964)910.
[41] T. Schaefer, S.R. Salman, T.A. Wildman, *J. Am. Chem. Soc*. 102 (1980)107.
[42] P. Retailleau, N. Colloc'h, D. Vivarès, F. Bonneté, B. Castro, M. El Hajji, J.P. Mornon, G. Monard, and T. Prangé, *Acta Cryst. Biol.Crystal.* 60(2004)453.
[43] E.J. Seo, H.J. Kim, M.J. Kim, J.S. Kim and J.B. Park. *Chem. Communi*. 55(2019)14462.